Power System Technology
ISSN:1000-3673

Received: 06-05-2024 *Revised: 15-06-2024* *Accepted: 28-07-2024*

Exploring the Effects of Inter-Particle Spacing and Nanoparticle Radius in The Flow Over a Rotating Exponentially Stretching Surface and Entropy Generation for Al_2O_3/H_2O Nanofluid

Behrooz Azizzadeh, Iraj Mirzaee, Morteza Khalilian*, Samad Jafarmadar

Mechanical Engineering Department, Faculty of Engineering, Urmia University, Urmia, Iran.

E-mail: be.azizzadeh@urmia.ac.ir

E-mail: i.mirzaee@urmia.ac.ir

(Corresponding author) E-mail: m.khalilian@urmia.ac.ir

E-mail: s.jafarmadar@urmia.ac.ir

Abstract

Nanofluids have found extensive industrial, engineering, and medical applications due to their increased heat transfer rate. A three-dimensional (3D) incompressible flow on rotating exponentially stretching surfaces was investigated for the water base fluid and aluminum oxide (Al_2O_3) nanoparticle. This study can be considered a novel analysis as it explores the effects of inter-particle spacing and nanoparticle radius on entropy generation, velocity, temperature, skin friction, Nusselt number (Nu), and Bejan number (Be) for an exponentially stretching flow. Partial differential equations (PDEs) are obtained using continuity, momentum, and energy equations. They are converted into three coupled ordinary differential equations (ODEs) by applying appropriate transformations. Numerical results and graphs are obtained using the bvp4c algorithm in MATLAB software. According to the results, the entropy generation rate decreases with increasing inter-particle spacing and increases with increasing nanoparticle radius. A comparison between the graphs demonstrates that the effect of inter-particle spacing and nanoparticle radius on Be is opposite to that of entropy generation. The entropy generation rate increases with increasing Ec. Moreover, Nu increases with increasing inter-particle spacing and decreases with increasing nanoparticle radius. As λ increases, temperature and entropy increase, and Be decreases.

Power System Technology
ISSN:1000-3673

Received: 06-05-2024 *Revised: 15-06-2024* *Accepted: 28-07-2024*

Keywords: Inter-particle spacing, Exponentially stretching, Nanoparticle radius, Entropy generation, bvp4c method

Introduction

Nowadays, it is widely acknowledged that thermal conductivity and other rheological properties of fluids can be increased by adding nanoparticles. Nanofluids have replaced ordinary fluids in most industrial applications and have dramatically altered their dynamics. Adding nanoparticles to fluids has led to reduced energy consumption and increased equipment lifespan. Nanofluids have found many applications in various fields, including engineering, space technologies, microelectronics, chillers, hybrid power engines, metallurgical industries, drug delivery, nuclear reactor coolants, heat exchangers, and cancer therapy. Many researchers have examined the thermophysical properties and characteristics of nanofluids in the last few decades from both conceptual and experimental perspectives.

The original concept of thermal efficiency-increasing nanoparticles was first introduced by Choi [1]. Junaid et al. [2] investigated the rotating nanofluid flow passing through a heated deformable surface. The base fluid was water, and the studied nanoparticles were copper oxide (CuO), copper (Cu), and silver (Ag). Governing differential equations were formulated nonlinearly, and the equations were solved using the 4th-order Runge-Kutta (RK4) method. Calculations indicated a direct relationship between skin friction and nanoparticle solid volume fraction. In addition, surface heat transfer rate was found to be an increasing function of nanoparticle solid volume fraction. Mustafa et al. [3] studied a 3D nanofluid flow over a linearly stretching surface with thermal radiation for water base fluid and Fe_3O_4 nanoparticles. Mustafa et al. [4] performed a numerical study on partial slip effects on magnetohydrodynamic (MHD) nanofluid flow near a stretchable rotating disk. Furthermore, the equations were simulated using the bvp4c technique. Shah et al. [5] analyzed the simultaneous magnetic and electric currents for nanofluid using the homotopy analysis method (HAM) solution between two rotating plates. Jyothi et al. [6] simulated the boundary layer flow and explored the slip effects for both stable and unstable states on stretching surfaces for the Au nanoparticle and kerosene base fluid. Ahmad et al. [7] surveyed the entropy generation for a nanofluid flow between two parallel plates for five different nanoparticles. Gholinia et al. [8] conducted a numerical simulation of fluid flow on a stretching cylinder for CNTs/$C_2H_6O_2$ hybrid nanofluid based on water base fluid in the presence of a magnetic field. Gholinia et al. [9] simulated a hybrid nanofluid flow on a cylinder with a sinusoidal radius using Akbari-Ganji's method (AGM) numerical method. Hayat et al. [10] investigated the flow over a rotating disk in the presence of thermal radiation for a nanofluid. For this purpose, the effect of Cu and Ag

Power System Technology
ISSN:1000-3673
Received: 06-05-2024 Revised: 15-06-2024 Accepted: 28-07-2024

nanoparticles on the thermal conductivity of the fluid was examined, and the entropy generation rate was calculated for different variables. Hayat et al. [11] studied a comparative model for a two-dimensional (2D) steady-state flow on stretchable curved surfaces. Hussain et al. [12] inspected a rotating nanofluid flow on a linearly stretching surface with partial slip. Hussain et al. [13] researched a 3D flow in the presence of a nonlinearly stretching magnetic field for water [base] nanofluid and zinc (Zn) and titanium oxide (TiO_2) nanoparticles. PDEs were converted into coupled ODEs by applying appropriate transformations. In addition, numerical results were obtained using the bvp4c algorithm in MATLAB software. Arshad et al. [14] looked into Brownian motion and thermophoresis effects for a 3D flow in the presence of a magnetic field. Ramzan et al. [15] examined a hybrid nanofluid flow between two parallel plates with convective boundary conditions. Hussain et al. [16] carried out a mathematical analysis of hybrid mediated blood flow in stenosis narrow arteries. Ramzan et al. [17] simulated the effect of inter-particle spacing and nanoparticle radius for a rotating disk flow on velocity, temperature, and Nusselt number (Nu), in the presence of a magnetic field. Studies have shown that the heat transfer rate of nanofluids is much higher than that of base fluids. Other studies have recently been conducted on nanofluids [18-24].

Incompressible fluid flow on rotating exponentially stretching surfaces has found many applications in engineering and industrial processes. Among the applications of boundary layer flow on stretched surfaces with linear and exponential functions in technical and engineering fields are aerodynamics, plastic sheet extrusion, food processing, glass fiber production, synthetic fibers, hot rolling, and stator/rotor parts. In each of the abovementioned cases, stretching velocity and heat transfer directly affect product quality and final shape. Many studies have been conducted on stretching surface flow [25-33].

Khan et al. [34] explored a 3D flow on a nonlinearly stretching sheet. The results indicated direct Brownian motion effects on temperature and heat transfer. Ahmed et al. [35] studied a nanofluid flow model with Cu, CuO, TiO_2, and aluminum oxide (Al_2O_3) nanoparticles on stretching surfaces with convective boundary conditions. The findings indicated the relative superiority of Al_2O_3 nanoparticles in heat transfer rate. Mushtaq et al. [36] explored the effects of velocity, temperature, and heat transfer rate on a rotating exponentially stretching plate. The results showed that nanofluid volume fraction is a key parameter in heat transfer rate. Hayat et al. [37] simulated a 3D incompressible second-grade nanofluid flow in the presence of a magnetic field. To this end, they analyzed velocity, temperature, skin friction, and Nu. According to the analysis, the temperature increased with increasing the magnetic parameter. Afridi et al. [38] examined a comparative model for nanofluid and hybrid nanofluid flowing over an exponentially stretching surface and entropy generation. Hussain et al. [39] performed

Power System Technology
ISSN:1000-3673
Received: 06-05-2024 Revised: 15-06-2024 Accepted: 28-07-2024

a numerical study on a hybrid nanofluid with CuO and TiO_2 nanoparticles over rotating exponentially stretching surfaces. Hussain et al. [40] analyzed a 3D rotating flow with slip boundary condition on exponentially stretching surfaces with Ag and CuO nanoparticles based on water base fluid.

The review of the above studies demonstrated that the effects of inter-particle spacing and nanoparticle radius in base fluid on entropy generation, velocity, temperature, Nu, and Bejan number (*Be*) in rotating flow with exponential stretching have not been examined yet. Moreover, considering the aforementioned applications for nanofluid flow over stretching surfaces, this research explored the effect of a 3D incompressible flow on a rotating exponentially stretching surface. Numerical results were obtained using the bvp4c algorithm in MATLAB software. According to the analysis, the entropy generation, temperature, skin friction, Nu, and Be graphs are highly dependent on essential parameters, including nanoparticle radius, inter-particle spacing, rotation, stretching, and Eckert number (*Ec*).

Mathematical model

Consider the steady, incompressible, three-dimensional and rotatig flow of dissipative nano fluid over an exponentially stretching surface, as depicted in Figure 1. The surface is extended in the x-direction, and the nanofluid flow is considered in the plane z > 0. The components of velocity along the x, y, and z axes are represented by u, v, and w respectively. The surface is stretched with an exponential function with velocity u_w and v_w. T is the tempruture, and T_∞ it the free stream tempreature. Whole system rotates along $z-axis$ with angular velocity ω. Consider Water (H_2O) act as a base liquid while Al_2O_3 as nanoparticle. The governing three-dimensional equations in the boundary layer flow are:

Continuity equations

$$\frac{\partial u}{\partial x}+\frac{\partial u}{\partial y}+\frac{\partial u}{\partial z}=0 \tag{1}$$

Momentum eguations

$$\rho_{nf}\left(u\frac{\partial u}{\partial x}+v\frac{\partial u}{\partial y}+w\frac{\partial u}{\partial z}\right)-2\omega v=\mu_{nf}\left(\frac{\partial^2 u}{\partial z^2}\right) \tag{2}$$

energy equations

Power System Technology
ISSN:1000-3673
Received: 06-05-2024 Revised: 15-06-2024 Accepted: 28-07-2024

$$\rho_{nf}\left(u\frac{\partial v}{\partial x}+v\frac{\partial v}{\partial y}+w\frac{\partial v}{\partial z}\right)+2\omega u=\mu_{nf}\left(\frac{\partial^2 v}{\partial z^2}\right) \tag{3}$$

$$\left(\rho c_p\right)_{nf}\left(u\frac{\partial T}{\partial x}+v\frac{\partial T}{\partial y}+w\frac{\partial T}{\partial z}\right)$$

$$=k_{nf}\left(\frac{\partial^2 T}{\partial z^2}\right)+\mu_{nf}\left[\left(\frac{\partial u}{\partial z}\right)^2+\left(\frac{\partial v}{\partial z}\right)^2\right] \tag{4}$$

Boundary conditions are as follows:

$$\mathrm{u}=u_w,\qquad \mathrm{v}=v_w,\qquad \mathrm{w}=0,$$

$$T=T_w,\qquad at\ \ z=0 \tag{5}$$

$$u\to 0,\qquad v\to 0,\qquad T\to T_\infty,\qquad as\quad z\to\infty \tag{6}$$

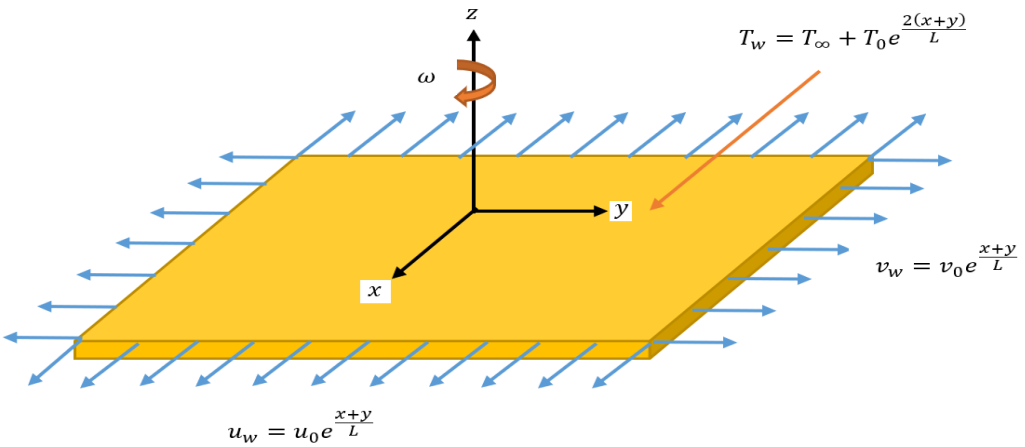

figure(1) The schematic diagram of the problem

Power System Technology
ISSN:1000-3673
Received: 06-05-2024 Revised: 15-06-2024 Accepted: 28-07-2024

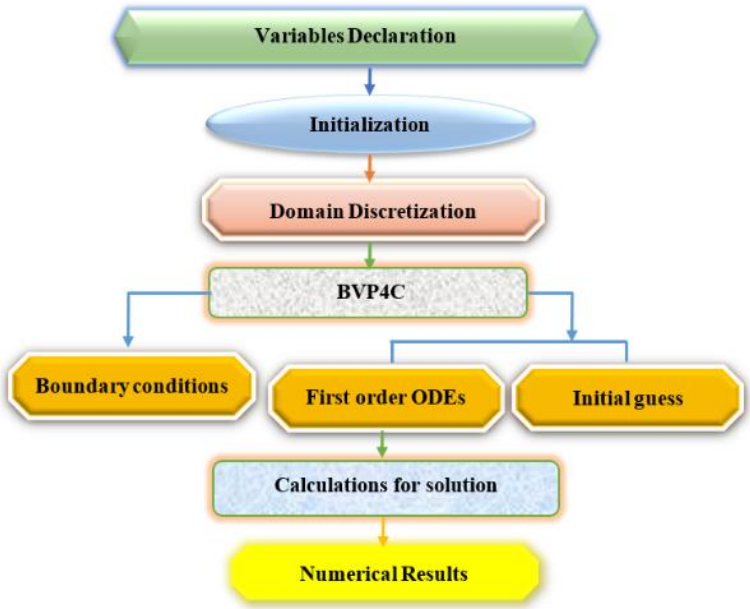

figure(2) flow chart of problem and method of solution

Theromophysical properties of nanofluid

This section introduces the thermophysical properties of Al_2O_3-H_2O nanofluid. Graham [41] and Gosukonda et al. [42] calculated the viscosity as follows:

$$\frac{\mu_{nf}}{\mu_f} = 1 + 2.5\Delta + 4.5\left[\frac{1}{\frac{h}{R_p}\left(2+\frac{h}{R_p}\right)\left(1+\frac{h}{R_p}\right)^2}\right] \tag{7}$$

where h, R_p, and Δ represent inter-particle spacing, nanoparticle radius, and solid volume fraction (SVF), respectively.

$$\rho_{nf} = (1-\Delta)\rho_f + \Delta\rho_{Al_2O_3} \tag{8}$$

$$\left(\rho C_p\right)_{nf} = (1-\Delta)(\rho C_p)_f + \Delta(\rho C_p)_{Al_2O_3} \tag{9}$$

$$\frac{k_{nf}}{k_f} = \frac{k_{Al_2O_3} + 2k_f - 2\Delta\left(k_f - k_{Al_2O_3}\right)}{k_{Al_2O_3} + 2k_f + \Delta\left(k_f - k_{Al_2O_3}\right)} \tag{10}$$

where ρ_{nf}, $\left(\rho C_p\right)_{nf}$, and k_{nf} denote the density, specific heat capacity, and thermal

Power System Technology
ISSN:1000-3673
Received: 06-05-2024 Revised: 15-06-2024 Accepted: 28-07-2024

conductivity of the nanofluid. Thermophysical properties of base the fluid and solid nanoparticle are shown in Table 1.

Table 1: Thermophysical properties of base the fluid and solid nanoparticle[17]

property	Bace fluid(H_2O)	Nano particle(Al_2O_3)
$C_p(J/kgK)$	4179	765
$k(W/mK)$	0.613	40
$\rho(kg/m^3)$	997.1	3970
Pr	7	-

The dimensionless quantities are

$$u_w = u_0 e^{\frac{x+y}{L}} \quad , v_w = v_0 e^{\frac{x+y}{L}} \quad , T_w = T_\infty + T_0 e^{\frac{2(x+y)}{L}} \tag{11}$$

Appropriate similarity transformations are as follows:

$$u = u_0 e^{\frac{x+y}{L}} f'(\eta) \ , v = v_0 e^{\frac{x+y}{L}} g'(\eta)$$

$$w = -\left(\frac{\upsilon u_0}{2L}\right) e^{\frac{(x+y)}{2L}} [f(\eta) + g(\eta) + f'(\eta) + g'(\eta)]$$

$$T = T_\infty + T_0 e^{\frac{2(x+y)}{L}} \theta(\eta) \ , \eta = z\left(\frac{u_0}{2\upsilon L}\right)^{\frac{1}{2}} e^{\frac{(x+y)}{2L}} \tag{12}$$

The continuity equation is satisfied by appropriate similarity transformations. Besides, the momentum and energy equations are simplified as follows:

$$\left(\frac{\mu_{nf}}{\mu_f}\right)\left(\frac{\rho_f}{\rho_{nf}}\right) f''' + f''(f+g) - 2f'(f'+g') + 4\lambda g' = 0 \tag{13}$$

Power System Technology
ISSN:1000-3673
Received: 06-05-2024 Revised: 15-06-2024 Accepted: 28-07-2024

$$\left(\frac{\mu_{nf}}{\mu_f}\right)\left(\frac{\rho_f}{\rho_{nf}}\right) g''' + g''(f+g) - 2f'(f'+g') - 4\lambda f' = 0 \tag{14}$$

$$\left(\frac{k_{nf}}{k_f}\right)\left(\frac{(\rho C_p)_f}{(\rho C_p)_{nf}}\right)\theta'' + Pr\theta'(f+g) - 4Pr\theta(f'+g') + EcPr\left(\frac{\mu_{nf}}{\mu_f}\right)\left(\frac{(\rho C_p)_f}{(\rho C_p)_{nf}}\right)(f''^2 + g''^2) = 0 \tag{15}$$

$$f(0) = 0,\ g(0) = 0,\quad f'(0) = 1,\ g'(0) = \beta \quad \theta(0) = 1 \quad at\ \eta = 0 \tag{16}$$

$$f' \to 0,\quad g' \to 0,\quad \theta \to 0,\quad as\ \eta \to \infty \tag{17}$$

$$Pr = \frac{\upsilon_f}{\alpha}, \beta = \frac{v_0}{u_0}, Ec = \frac{{u_w}^2}{(C_p)_f T_0}, \lambda = \frac{\omega L}{u_0} \tag{18}$$

In addition, skin friction and *Nu* are calculated as follows:

$$C_{fx} = \frac{\tau_{wx}}{\frac{1}{2}\rho_f {u_w}^2},\ C_{fy} = \frac{\tau_{wy}}{\frac{1}{2}\rho_f {u_w}^2},\ Nu_x = \frac{x q_w}{k_f(T_w - T_\infty)} \tag{19}$$

The wall shear stresses τ_{wx}, τ_{wy} and heat flux q_w expressions are

$$\tau_{wx} = \mu_{nf}\left(\frac{\partial u}{\partial z}\right)_{z=0}, \tau_{wy} = \mu_{nf}\left(\frac{\partial v}{\partial z}\right)_{z=0} \quad q_w = k_{nf}\left(\frac{\partial T}{\partial z}\right)_{z=0} \tag{20}$$

Now, using Eqs. (12) and (20) in (19), we get

$$\frac{1}{\sqrt{2}} C_{fx}\, {Re_x}^{\frac{1}{2}} = \frac{1}{(1-\Delta)^{2.5}} f''(0) \quad \frac{1}{\sqrt{2}} C_{fy}\, {Re_x}^{\frac{1}{2}} = \frac{1}{(1-\Delta)^{2.5}} g''(0) \tag{21}$$

Power System Technology
ISSN:1000-3673
Received: 06-05-2024 Revised: 15-06-2024 Accepted: 28-07-2024

$$\sqrt{2}\frac{L}{x}Nu_x Re_x^{-\frac{1}{2}} = -\frac{k_{nf}}{k_f}\theta'(0)$$

Entropy formulation

Afridi et al. [38] calculated the entropy generation rate as:

$$\dot{S}_{Gen}''' = \frac{k_{nf}}{T^2}\left(\frac{\partial T}{\partial z}\right)^2 + \frac{\mu_{nf}}{T}\left[\left(\frac{\partial u}{\partial z}\right)^2 + \left(\frac{\partial v}{\partial z}\right)^2\right] \quad (22)$$

$$(\dot{S}_{Gen}''')_0 = \frac{k_f u_w}{2v_f L} \quad (23)$$

The entropy generation rate is calculated using Eqs. (22) and (23) as well as similarity transformations:

$$\mathrm{Ns} = \frac{\dot{S}_{Gen}'''}{(\dot{S}_{Gen}''')_0} = \left(\frac{k_{nf}}{k_f}\right)\frac{\theta'^2}{(\theta + \Omega)^2} + \left(\frac{\mu_{nf}}{\mu_f}\right)\frac{EcPr}{(\theta + \Omega)}(f''^2 + g''^2) \quad (24)$$

where $\Omega = T_\infty/(T_w - T_\infty)$ denotes the temperature difference.

Be (irreversibility parameter) can be defined as follows:

$$Be = \frac{(k_{nf}/T^2)(\partial T/\partial y)^2}{(k_{nf}/T^2)(\partial T/\partial y)^2 + (\mu_{nf}/T)[(\partial u/\partial z)^2 + (\partial v/\partial z)^2]} \quad (25)$$

Be is calculated using similarity transformations as:

$$\mathrm{Be} = k_{nf}(\mu_f/\mu_{nf})\theta'^2 / \left(k_{nf}(\mu_f/\mu_{nf})\theta'^2 + EcPrk_f(\theta + \Omega)(f''^2 + g''^2)\right) \quad (26)$$

Power System Technology
ISSN:1000-3673
Received: 06-05-2024 Revised: 15-06-2024 Accepted: 28-07-2024

Numerical approach

The transformed ordinary differential Eqs. (13)-(15) are solved numerically by using the MATLAB bvp4c algorithm. The highly non-linear Eqs. (13)-(15) are transformed into first-order ODEs using a new set of variables. Figure 2 shows a graphical representation of the entire algorithm. Following this, suitable initial guesses are selected to satisfy the boundary conditions. A convergence criterion of 10^ (-6) is set for the obtained solution. The following are the new variables. Figure 3 shows a Flow chart of the numerical solution method. The bvp-4c algorithm is a numerical code for solving a set of differential equations in Matlab software.

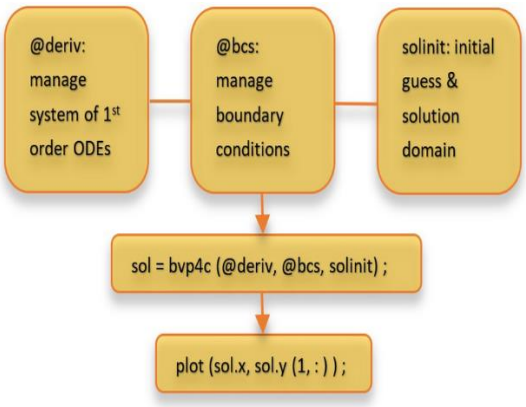

Figure 3. Flow chart for bvp-4c

$$y_1 = f, \quad y_2 = f', \quad y_3 = f'', \quad y_3' = f''',$$
$$y_4 = g, \quad y_5 = g', \quad y_6 = g'', \quad y_6' = g''',$$
$$y_7 = \theta, \quad y_8 = \theta', \quad y_8' = \theta'', \tag{27}$$

A new set of variables are difined as follows in MATLAB to obtain the numerical solution.

$$y_1' = y_2 \tag{28}$$

$$y_2' = y_3 \tag{29}$$

$$y_3' = \left(\frac{\mu_f}{\mu_{nf}}\right)\left(\frac{\rho_{nf}}{\rho_f}\right)[2\,y_2(y_2 + y_5) - y_3(y_1 + y_4) - 4\lambda y_5\,] \tag{30}$$

Power System Technology
ISSN:1000-3673
Received: 06-05-2024 Revised: 15-06-2024 Accepted: 28-07-2024

$$y_4' = y_5 \tag{31}$$

$$y_5' = y_6 \tag{32}$$

$$y_6' = \left(\frac{\mu_f}{\mu_{nf}}\right)\left(\frac{\rho_{nf}}{\rho_f}\right)[2\,y_5(y_2 + y_5) - y_6(y_1 + y_4) + 4\lambda y_2\,] \tag{33}$$

$$y_7' = y_8 \tag{34}$$

$$y_8' = Pr\left(\frac{k_f}{k_{nf}}\right)\left(\frac{(\rho C_p)_{nf}}{(\rho C_p)_f}\right)\left[4y_7(y_2 + y_5) - y_8(y_1 + y_4) - Ec\left(\frac{\mu_{nf}}{\mu_f}\right)\left(\frac{(\rho C_p)_f}{(\rho C_p)_{nf}}\right)({y_3}^2 + {y_6}^2)\right] \tag{35}$$

The transformed boundary conditions changed in to the subsequent form:

$$y_1(a) = 0,\ \ y_2(a) = 1,\ \ y_4(a) = 0,\ \ y_5(a) = \beta,\ \ y_7(a) = 1 \tag{36}$$

$$y_2(b) = 0,\ \ y_5(b) = 0,\ \ y_4(b) = 0 \tag{37}$$

The skin friction and Nusselt number changed into the following form:

$$\frac{1}{\sqrt{2}} C_{fx}\, {Re_x}^{\frac{1}{2}} = \frac{1}{(1-\Delta)^{2.5}}\, y_3(0)$$

$$\frac{1}{\sqrt{2}} C_{fy}\, {Re_x}^{\frac{1}{2}} = \frac{1}{(1-\Delta)^{2.5}}\, y_6(0) \tag{38}$$

$$\sqrt{2}\frac{L}{x} Nu_x {Re_x}^{-\frac{1}{2}} = -\frac{k_{nf}}{k_f}\, y_8(0)$$

Also Be number and Ns with transformation becomes

Power System Technology
ISSN:1000-3673
Received: 06-05-2024 Revised: 15-06-2024 Accepted: 28-07-2024

$$\mathrm{Ns} = \left(\frac{k_{nf}}{k_f}\right)\frac{{y_8}^2}{(y_7 + \Omega)^2} + \left(\frac{\mu_{nf}}{\mu_f}\right)\frac{EcPr}{(y_7 + \Omega)}({y_3}^2 + {y_6}^2) \quad (39)$$

$$\mathrm{Be} = k_{nf}(\mu_f/\mu_{nf}){y_8}^2 / \left(k_{nf}(\mu_f/\mu_{nf}){y_8}^2 + EcPrk_f(y_7 + \Omega)({y_3}^2 + {y_6}^2)\right) \quad (40)$$

Analysis of Results

This section demonstrates the parameters of the velocity components $f'(\eta)$ (axial velocity), $g'(\eta)$ (transverse velocity), temperature distribution $\theta(\eta)$, entropy generation, *Be*, skin friction, and Nu in different graphs, and discusses in detail their changes with respect to different parameters. Table 2 presents the results of a numerical comparison between $-f''(0)$ and $-g''(0)$ parameters using the bvp4c and shooting techniques. The results obtained from both methods are in good agreement, confirming the numerical method used.

Table 2: Comparison of the numerical results of $-f''(0)\ and\ -g''(0)$ for different values of β

	Bvp4c		Shooting	
β	$-f''(0)$	$-g''(0)$	$-f''(0)$	$-g''(0)$
0.3	1.14941	0.48978	1.14942	0.48977
0.6	1.24930	0.91498	1.24930	0.91498
0.9	1.34053	1.41080	1.34052	1.41081

Fig. 4 explores the effect of β on $f'(\eta)$ for both h=0.5 and h=1.5 states. As can be seen, $f'(\eta)$ decreases with increasing β for both h=0.5 and h=1.5 states, which can be justified by the value of $\beta = \frac{v_0}{u_0}$. According to this equation, the velocity in the x-direction (horizontal velocity) decreases as β increases. Also, $f'(\eta)$ decreases for higher h values.The effect of β on $f'(\eta)$ for both R_p=1 and R_p=2 states is displayed in Fig. 5. As can be seen, for both R_p=1 and R_p=2 states, $f'(\eta)$ decreases with increasing β and increases for higher R_p values.Fig. 6 represents the effect of R_p on $f'(\eta)$ for both h=0.5 and h=1.5 states. As can be seen, for both

Power System Technology
ISSN:1000-3673
Received: 06-05-2024 Revised: 15-06-2024 Accepted: 28-07-2024

h=0.5 and h=1.5 states, $f'(\eta)$ increases with increasing R_p and decreases for higher h values. Fig. 7 plots the effect of β on $g'(\eta)$ for both h=0.5 and h=1.5 states. As can be seen, $g'(\eta)$ increases with increasing β for both h=0.5 and h=1.5 states, which can be justified by the value of $\beta = \frac{v_0}{u_0}$. According to this equation, the velocity in the y-direction (vertical velocity) increases with increasing β. Also, $g'(\eta)$ decreases for higher h values. The effect of β on $g'(\eta)$ for both R_p=1 and R_p=2 states is showed in Fig. 8 . As can be seen, for both R_p=1 and R_p=2 states, $g'(\eta)$ increases with increasing β and increases for higher R_p values. Fig. 9 displays the effect of R_p on $g'(\eta)$ for both h=0.5 and h=1.5 states. As can be seen, for both h=0.5 and h=1.5 states, $g'(\eta)$ increases with increasing R_p and decreases for higher h values.

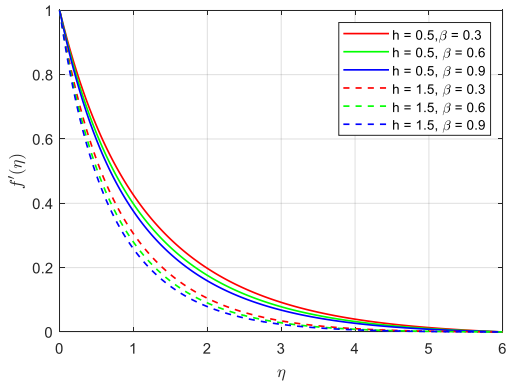

figure(4) Influence of β on the velocity $f'(\eta)$ when $h = 0.5$ *and* $h = 1.5$

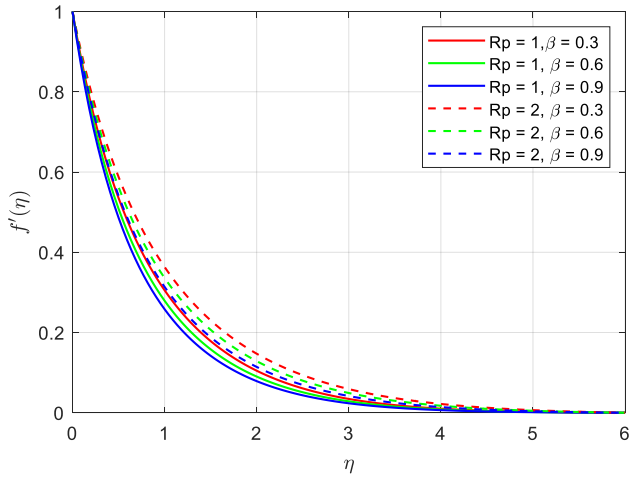

figure(5) Influence of β on the velocity $f'(\eta)$ when $R_p = 1$ *and* $R_p = 2$

Power System Technology
ISSN:1000-3673
Received: 06-05-2024 Revised: 15-06-2024 Accepted: 28-07-2024

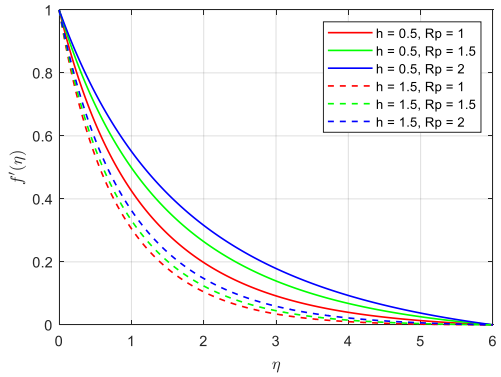

figure(6) Influence of R_p on the velocity $f'(\eta)$ when $h = 0.5$ *and* $h = 1.5$

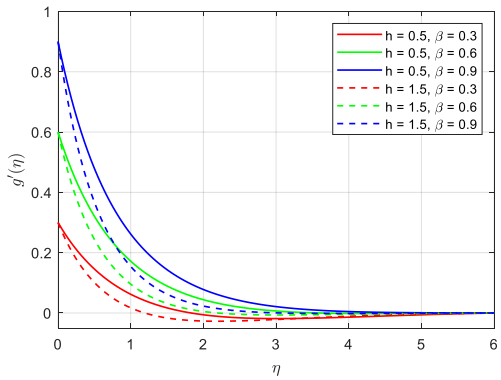

figure(7) Influence of β on the velocity $g'(\eta)$ when $h = 0.5$ *and* $h = 1.5$

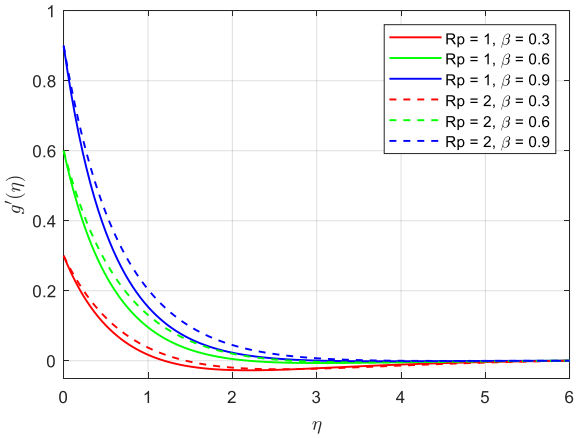

figure(8) Influence of β on the velocity $g'(\eta)$ when $R_p = 1$ *and* $R_p = 2$

Power System Technology
ISSN:1000-3673
Received: 06-05-2024 Revised: 15-06-2024 Accepted: 28-07-2024

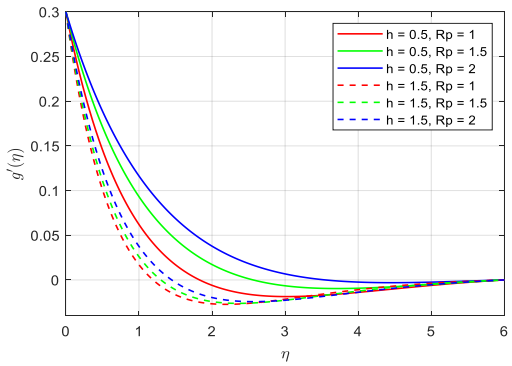

figure(9) Influence of R_p on the velocity $g'(\eta)$ when $h = 0.5$ *and* $h = 1.5$

Fig. 10 investigate the effect of Rp on $\theta(\eta)$ for both h=0.5 and h=1.5 states. As can be seen, for both h=0.5 and h=1.5 states, $\theta(\eta)$ increases with increasing Rp and decreases for higher h values. According to the above graph, the highest and lowest $\theta(\eta)$ are obtained when Rp=2 and h=0.5 and Rp=1 and h=1.5, respectively. This indicates the highest temperature for higher nanoparticle radius and lower inter-particle spacing, and the lowest temperature for lower nanoparticle radius and higher inter-particle spacing. Physically, when the distance between the nanoparticles is small and the radius of the nanoparticles is large, there is more intermolecular collision, which results in an increase in temperature. The effect of λ on $\theta(\eta)$ for both Ec=0.5 and Ec=1 states is explored in Fig. 11. As can be seen, for both Ec=0.5 and Ec=1 states, $\theta(\eta)$ increases with increasing λ and for higher Ec values. The scientific reason behind this analysis is that heat transfer increases with increasing Ec, resulting in increased thermal boundary layer thickness and temperature. An increase in the Eckert number means an increase in kinetic energy and, as a result, an increase in thermal energy.

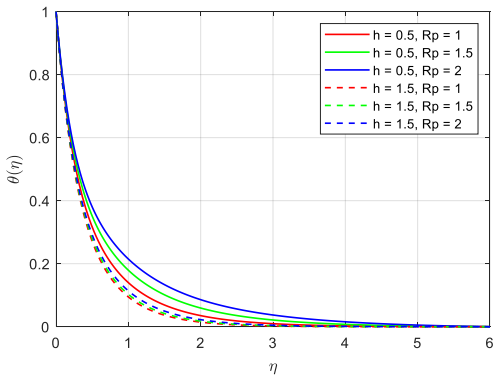

figure(10) Influence of R_p on the temperature $\theta(\eta)$ when $h = 0.5$ *and* $h = 1.5$

Power System Technology
ISSN:1000-3673
Received: 06-05-2024 Revised: 15-06-2024 Accepted: 28-07-2024

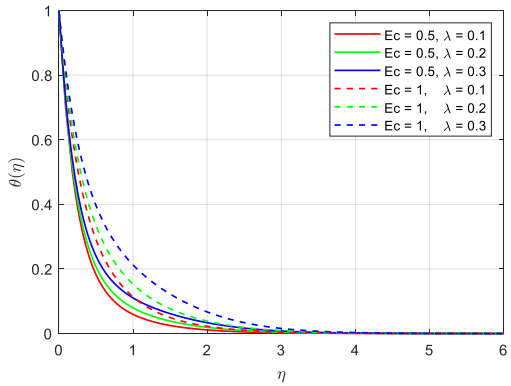

figure(11) Influence of Ec on the temperature $\theta(\eta)$ when $Ec = 0.5$ and $Ec = 1$

Fig. 12 indicates the effect of Ec on Ns for both h=0.5 and h=1.5 states. As can be seen, the entropy generation rate increases with increasing Ec for both h=0.5 and h=1.5 states. The scientific reason behind this analysis is that heat transfer increases with increasing Ec, leading to a higher entropy generation rate. Moreover, the entropy generation rate decreases with increasing inter-particle spacing. This indicates the highest entropy generation rate for higher Ec and lower inter-particle spacing and the lowest entropy generation rate for lower Ec and higher inter-particle spacing. As the Eckert number increases, the kinetic energy of the nanofluid increases, and as a result, the thermal energy increases and finally the entropy increases. When the distance between the nanoparticles is small, the intermolecular collision and friction are more, resulting in more entropy.

Fig. 13 illustrates the effect of Ec on Ns for both Rp=1 and Rp=2 states. As can be seen, the entropy generation rate increases with increasing Ec for both Rp=1 and Rp=2 states. The scientific reason behind this analysis is that heat transfer increases with increasing Ec, leading to a higher entropy generation rate. Besides, the entropy generation rate increases with increasing nanoparticle radius. This indicates the highest entropy generation rate for higher Ec and nanoparticle radius and the lowest entropy generation rate for lower Ec and nanoparticle radius. When the radius of nanoparticles is large. More intermolecular collisions and friction result in more entropy generation. The effect of R_p on Ns for both h=0.5 and h=1.5 states is discussed in Fig. 14 . As can be seen, for both h=0.5 and h=1.5 states, the entropy generation rate increases with increasing R_p and decreases with increasing inter-particle spacing. This indicates the highest entropy generation rate for higher nanoparticle radius and lower inter-particle spacing, and the lowest entropy generation rate for lower nanoparticle radius and higher inter-particle spacing. Physically, when the distance between the nanoparticles is small and the radius of the nanoparticles is large, there is more intermolecular collision, which results

Power System Technology
ISSN:1000-3673
Received: 06-05-2024 Revised: 15-06-2024 Accepted: 28-07-2024

in an increase in entropy generation. Fig. 15 investigate the effect of β on Ns for both h=0.5 and h=1.5 states. As can be seen, for both h=0.5 and h=1.5 states, the entropy generation rate increases with increasing β and decreases with increasing the inter-particle spacing. To reduce the entropy, the stretching parameter should be reduced and the distance between the nanoparticles should be increased. Fig. 16 is organized to describe the effect of λ on Ns for both Rp=1 and Rp=2 states. As can be seen, the entropy generation rate increases with increasing λ for both Rp=1 and Rp=2 states. As the rotation parameter increases, irreversibility increases and thus entropy generation increases.

The effect of λ on Ns for both Ec=0.5 and Ec=1 states is depicted in Fig. 17. As can be seen, for both Ec=0.5 and Ec=1 states, the entropy generation rate increases with increasing λ and Ec. The highest entropy production occurs for higher Eckert number and rotation parameter. Physically, both have an increasing role in entropy generation. Fig. 18 explores the effect of Ω on Ns for both R_p=1 and R_p=2 states. As can be seen, for both R_p=1 and R_p=2 states, the entropy generation rate decreases with increasing Ω and increases with increasing the nanoparticle radius.

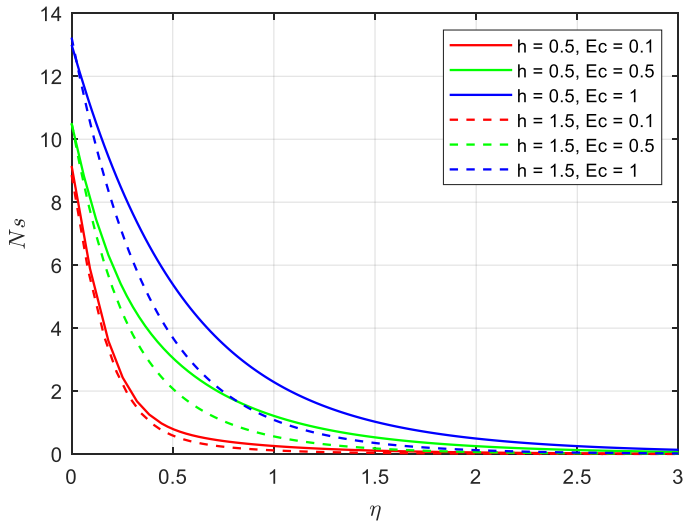

figure(12) Influence of Ec on the temperature Ns when $h = 0.5$ and $h = 1.5$

Power System Technology
ISSN:1000-3673
Received: 06-05-2024 Revised: 15-06-2024 Accepted: 28-07-2024

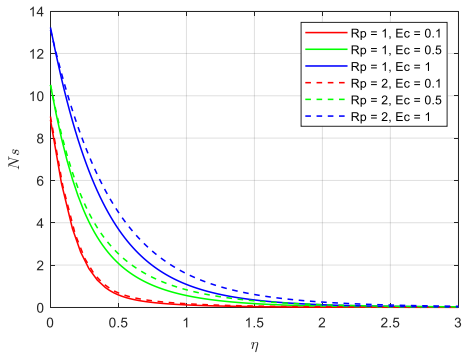

figure(13) Influence of Ec on the temperature Ns when $R_p = 1$ and $R_p = 2$

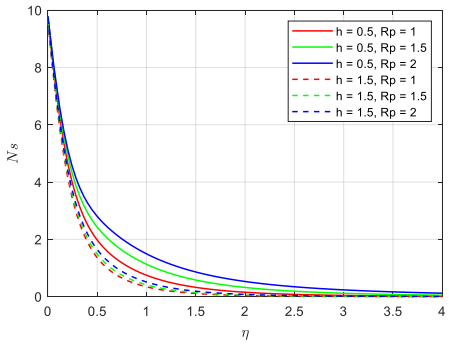

figure(14) Influence of Rp on the temperature Ns when $h = 0.5$ and $h = 1.5$

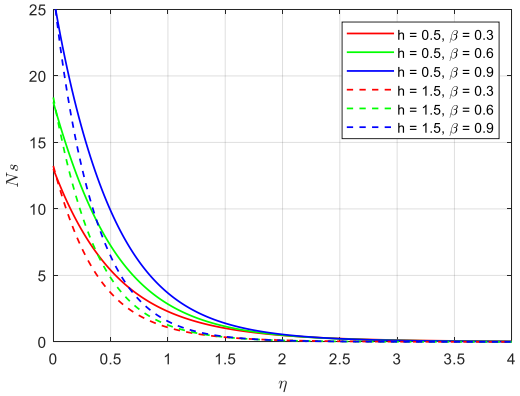

figure(15) Influence of β on the temperature Ns when $h = 0.5$ and $h = 1.5$

Power System Technology
ISSN:1000-3673
Received: 06-05-2024 Revised: 15-06-2024 Accepted: 28-07-2024

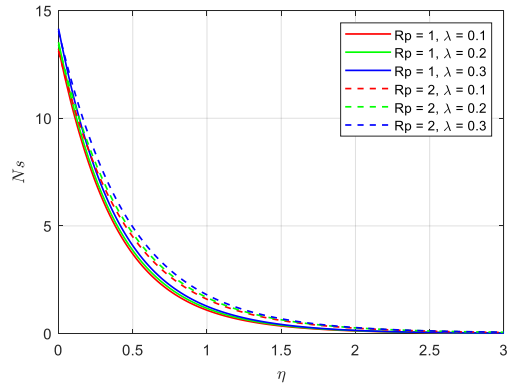

figure(16) Influence of λ on the temperature Ns when $Rp = 1$ and $Rp = 2$

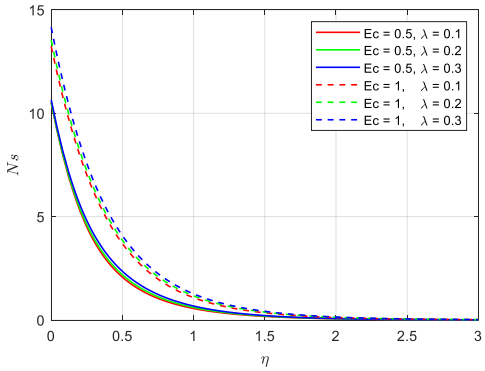

figure(17) Influence of λ on the temperature Ns when $Ec = 0.5$ and $Ec = 1$

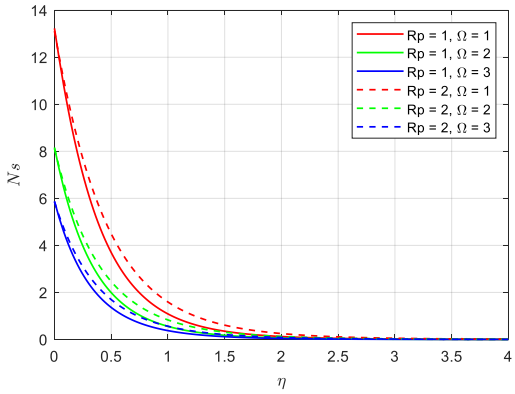

figure(18) Influence of Ω on the temperature Ns when $Rp = 1$ and $Rp = 2$

Power System Technology
ISSN:1000-3673
Received: 06-05-2024 Revised: 15-06-2024 Accepted: 28-07-2024

Fig. 19 represents the effect of *Ec* on *Be* for both *h*=0.5 and *h*=1.5 states. As can be seen, for both *h*=0.5 and *h*=1.5 states, *Be* decreases with increasing *Ec* and increases with increasing the inter-particle spacing. The reduced *Be* indicates a lower contribution of heat transfer in entropy generation compared to fluid friction. The effect of Rp on Be for both h=0.5 and h=1.5 states is displayed in Fig. 20. As can be seen, for both h=0.5 and h=1.5 states, Be decreases with increasing Rp and increases with increasing the inter-particle spacing. Physically, when the distance between the nanoparticles is large and the radius of the nanoparticles is small. The contribution of friction in the entropy generation decreases and as a result the Bejan number increases. Fig. 21 portrays the effect of β on *Be* for both R_p=1 and R_p=2 states. As can be seen, for both R_p=1 and R_p=2 states, *Be* decreases with increasing β and nanoparticle radius. To increase the Bejan number, the stretching parameter and the radius of the nanoparticles should be reduced. The reason for this increase, is the decrease in entropy generated by nanofluid friction. Fig. 22 describes the effect of λ on *Be* for both *Ec*=0.5 and *Ec*=1 states. As can be seen, for both *Ec*=0.5 and *Ec*=1 states, *Be* decreases with increasing λ and *Ec*. The effect of Ω on Be for both R_p=1 and R_p=2 states is analyzed in Fig. 23 . As can be seen, for both R_p=1 and R_p=2 states, *Be* decreases with increasing Ω and nanoparticle radius.

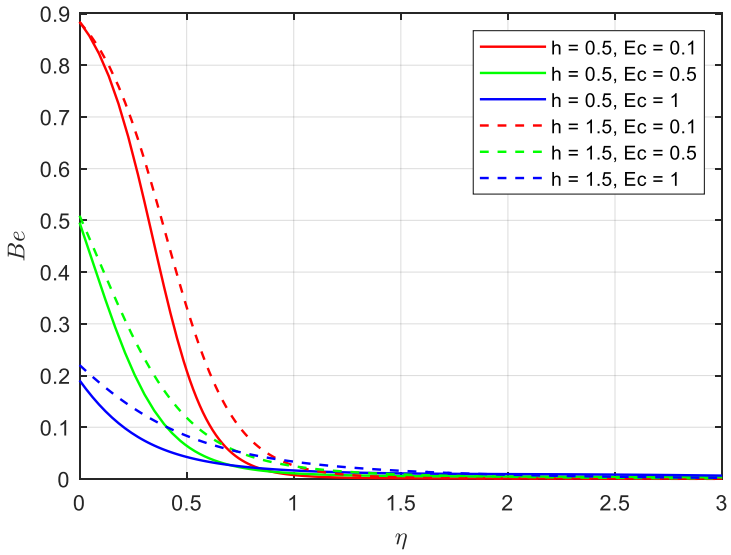

figure(19) Influence of Ec on the temperature Be when $h = 0.5$ and $h = 1.5$

Power System Technology
ISSN:1000-3673
Received: 06-05-2024 Revised: 15-06-2024 Accepted: 28-07-2024

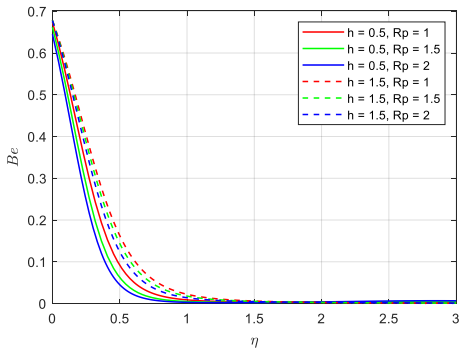

figure(20) Influence of Rp on the temperature Be when $h = 0.5$ and $h = 1.5$

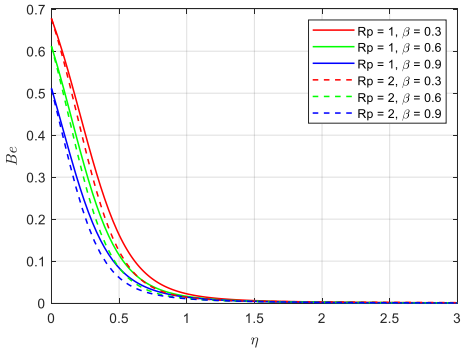

figure(21) Influence of β on the velocity Be when $R_p = 1$ and $R_p = 2$

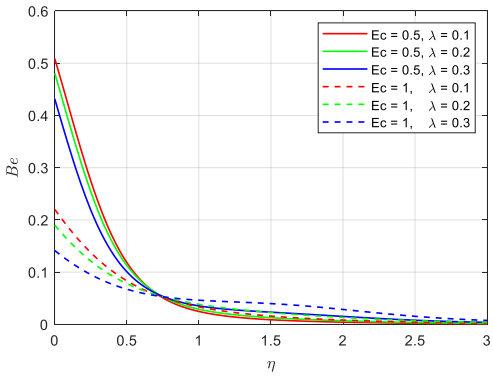

figure(22) Influence of λ on the temperature Be when $Ec = 0.5$ and $Ec = 1$

Power System Technology
ISSN:1000-3673
Received: 06-05-2024 Revised: 15-06-2024 Accepted: 28-07-2024

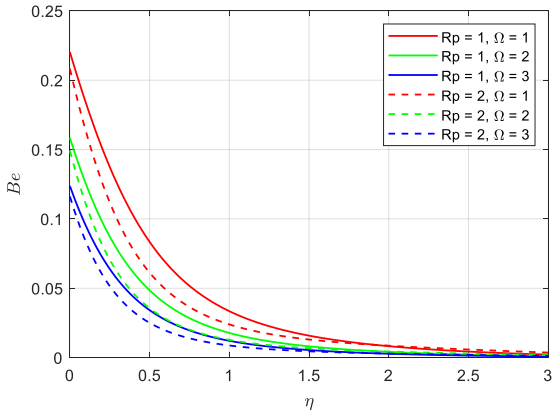

figure(23) Influence of Ω on the Be when $Rp = 1$ and $Rp = 2$

Conclusions

This research discussed a rotating 3D flow on an exponentially stretching surface for the Al_2O_3-H_2O nanofluid. For this purpose, the velocity, temperature, skin friction, *Nu*, entropy, and *Be* graphs were compared for different states.

The results of the main analysis can be summarized as follows:

1) In exploring the effect of β for both h=0.5 and h=1.5 states, $f'(\eta)$ decreased and $g'(\eta)$ increased with increasing β and for higher h values.

2) In exploring the effect of β for both R_p=1 and R_p=2 states, $f'(\eta)$ decreased and $g'(\eta)$ increased with increasing β, while $f'(\eta)$ and $g'(\eta)$ increased for higher R_p values.

3) In exploring the effect of R_p for both h=0.5 and h=1.5 states, $f'(\eta)$ and $g'(\eta)$ increased with increasing R_p, while they decreased for higher h values.

4) The highest temperature was obtained for higher nanoparticle radius and lower inter-particle spacing, while the lowest temperature was obtained for lower nanoparticle radius and higher inter-particle spacing.

5) For both h=0.5 and h=1.5 states, the entropy generation rate increased with increasing *Ec*, whereas it decreased with increasing the inter-particle spacing.

6) For both R_p=1 and R_p=2 states, the entropy generation rate increased with increasing *Ec* and nanoparticle radius.

Power System Technology
ISSN:1000-3673
Received: 06-05-2024 Revised: 15-06-2024 Accepted: 28-07-2024

7) Temperature and entropy generation increased and *Be* decreased with increasing λ.

8) The highest entropy generation rate was obtained for higher nanoparticle radius and lower inter-particle spacing, while the lowest entropy generation rate was obtained for lower nanoparticle radius and higher inter-particle spacing.

9) *Be* increased with increasing the inter-particle spacing, while it decreased with increasing the nanoparticle radius.

10) For both h=0.5 and h=1.5 states, C_{fx} and C_{fy} increased with increasing R_p and decreased with increasing h.

11) For both h=0.5 and h=1.5 states, Nu_x decreased with increasing β and nanoparticle radius, while it increased with increasing the inter-particle spacing.

References

[1]S.U. Choi, J.A. Eastman, Enhancing thermal conductivity of fluids with nanoparticles, in, Argonne National Lab.(ANL), Argonne, IL (United States), 1995.

[2]J.A. Khan, M. Mustafa, A. Mushtaq, On three-dimensional flow of nanofluids past a convectively heated deformable surface: A numerical study, International Journal of Heat and Mass Transfer, 94 (2016) 49-55.

[3]M. Mustafa, A. Mushtaq, T. Hayat, A. Alsaedi, Rotating flow of magnetite-water nanofluid over a stretching surface inspired by non-linear thermal radiation, Plos One, 11(2) (2016) e0149304.

[4]M. Mustafa, J.A. Khan, Numerical study of partial slip effects on MHD flow of nanofluids near a convectively heated stretchable rotating disk, Journal of Molecular Liquids, 234 (2017) 287-295.

[5]Z .Shah, S. Islam, T. Gul, E. Bonyah, M.A. Khan, The electrical MHD and hall current impact on micropolar nanofluid flow between rotating parallel plates, Results in physics, 9 (2018) 1201-1214.

[6]K. Jyothi, P. Sudarsana Reddy, M.R. Suryanarayana Reddy, B .Prabhavathi, Impact of slip effects on unsteady Sisko nanoliquid heat and mass transfer characteristics over stretching sheet filled with gold nanoparticles, Heat Transfer, 49(4) (2020) 2103-2130.

[7]S. Ahmad, M.I. Khan, T. Hayat, M.I. Khan, A. Alsaedi ,Entropy generation optimization and unsteady squeezing flow of viscous fluid with five different shapes of nanoparticles, Colloids and Surfaces A: Physicochemical and Engineering Aspects, 554 (2018) 197-210.

Power System Technology
ISSN:1000-3673
Received: 06-05-2024 Revised: 15-06-2024 Accepted: 28-07-2024

[8]M. Gholinia, M. Armin, A. Ranjbar, D. Ganji, Numerical thermal study on CNTs/C2H6O2–H2O hybrid base nanofluid upon a porous stretching cylinder under impact of magnetic source, Case Studies in Thermal Engineering, 14 (2019) 100490.

[9]M. Gholinia, K. Hosseinzadeh, D. Ganji, Investigation of different base fluids suspend by CNTs hybrid nanoparticle over a vertical circular cylinder with sinusoidal radius, Case Studies in Thermal Engineering, 21 (2020) 100666.

[10]T. Hayat, M.I. Khan, S. Qayyum, A. Alsaedi, Entropy generation in flow with silver and copper nanoparticles, Colloids and Surfaces A: Physicochemical and Engineering Aspects, 539 (2018) 335-346.

[11]T. Hayat, A. Kiran, M. Imtiaz, A. Alsaedi, Hydromagnetic mixed convection flow of copper and silver water nanofluids due to a curved stretching sheet, Results in physics, 6 (2016) 904-910.

[12]A. Hussain, M. Arshad, A. Hassan, A. Rehman, H. Ahmad, J. Baili, T.N. Gia, Heat transport investigation of engine oil based rotating nanomaterial liquid flow in the existence of partial slip effect ,Case Studies in Thermal Engineering, 28 (2021) 101500.

[13]A. Hussain, M. Arshad, A. Rehman, A. Hassan, S. Elagan, H. Ahmad, A. Ishan, Three-dimensional water-based magneto-hydrodynamic rotating nanofluid flow over a linear extending sheet and heat transport analysis: A numerical approach, Energies, 14(16) (2021) 5133.

[14]M. Arshad, A. Hussain, A. Hassan, Q. Haider, A.H. Ibrahim, M.S. Alqurashi, A.H. Almaliki, A. Abdussattar, Thermophoresis and brownian effect for chemically reacting magneto-hydrodynamic nanofluid flow across an exponentially stretching sheet, Energies, 15(1) (2021) 143.

[15]M. Ramzan, N. Shahmir, H.A.S. Ghazwani, K.S. Nisar, F.M. Alharbi, I. Yahia, Hydrodynamic and heat transfer analysis of dissimilar shaped nanoparticles-based hybrid nanofluids in a rotating frame with convective boundary condition, Scientific Reports, 12(1) (2022) 436.

[16]A. Hussain, L. Sarwar, A. Rehman, Q. Al Mdallal, A.H. Almaliki, A. El-Shafay, Mathematical analysis of hybrid mediated blood flow in stenosis narrow arteries, Scientific reports, 12(1) (2022) 12704.

[17]M. Ramzan, S.A. Lone, A. Dawar, A. Saeed, W. Kumam, P. Kumam, Significance of nanoparticle radius and inter-particle spacing toward the radiative water-based alumina nanofluid flow over a rotating disk, Nanotechnology Reviews, 12(1) (2023) 20220501.

[18]M. Ramzan, A. Dawar, A. Saeed, P. Kumam, K. Sitthithakerngkiet, S.A. Lone, Analysis of the partially ionized kerosene oil-based ternary nanofluid flow over a convectively heated rotating surface, Open Physics, 20(1) (2022) 507-525.

[19]M. Ramzan, N.S. Khan, P. Kumam, Mechanical analysis of non-Newtonian nanofluid past

Power System Technology
ISSN:1000-3673
Received: 06-05-2024 Revised: 15-06-2024 Accepted: 28-07-2024

a thin needle with dipole effect and entropic characteristics, Scientific Reports, 11(1) (2021) 19378.

[20]A. Dawar, A. Saeed ,P. Kumam, Magneto-hydrothermal analysis of copper and copper oxide nanoparticles between two parallel plates with Brownian motion and thermophoresis effects, International Communications in Heat and Mass Transfer, 133 (2022) 105982.

[21]M. Hafeez, T. Hayat, A. Alsaedi, M.I. Khan, Numerical simulation for electrical conducting rotating flow of Au (Gold)-Zn (Zinc)/EG (Ethylene glycol) hybrid nanofluid, International Communications in Heat and Mass Transfer, 124 (2021) 105234.

[22]F.N. Jamrus, I. Waini, U .Khan, A. Ishak, Effects of magnetohydrodynamics and velocity slip on mixed convective flow of thermally stratified ternary hybrid nanofluid over a stretching/shrinking sheet, Case Studies in Thermal Engineering, (2024) 104161.

[23]B. Ali, S. Jubair, A .Aluraikan, M. Abd El-Rahman, S.M. Eldin, H.A.E.-W. Khalifa, Numerical investigation of heat source induced thermal slip effect on trihybrid nanofluid flow over a stretching surface, Results in Engineering, 20 (2023) 101536.

[24]S. Muhammad Raza Shah Naqvi, U. Manzoor, H. Waqas, D. Liu, H. Naeem, S.M. Eldin, T. Muhammad, Numerical investigation of thermal radiation with entropy generation effects in hybrid nanofluid flow over a shrinking/stretching sheet, Nanotechnology Reviews, 13(1) (2024) 20230171.

[25]A.J. Chamkha, C. Issa, Mixed convection effects on unsteady flow and heat transfer over a stretched surface, International communications in heat and mass transfer, 26(5) (1999) 717-727.

[26]K.L. Hsiao, MHD stagnation point viscoelastic fluid flow and heat transfer on a thermal forming stretching sheet with viscous dissipation, the Canadian journal of chemical engineering, 89(5) (2011) 1228-1235.

[27]N.A. Khan, F. Sultan, Homogeneous-heterogeneous reactions in an Eyring-Powell fluid over a stretching sheet in a porous medium, Special Topics & Reviews in Porous Media: An International Journal, 7(1.(2016) (

[28]Z. Khan, M. Qasim, N. Ishfaq, W. Khan, Dual solutions of MHD boundary layer flow of a micropolar fluid with weak concentration over a stretching/shrinking sheet, Communications in Theoretical Physics, 67(4) (2017) 449.

[29]K. Prasad, K. Vajravelu, P. Datti, Mixed convection heat transfer over a non-linear stretching surface with variable fluid properties, International Journal of non-linear Mechanics, 45(3) (2010) 320-330.

[30]M. Turkyilmazoglu, Analytic heat and mass transfer of the mixed hydrodynamic/thermal slip MHD viscous flow over a stretching sheet, International Journal of Mechanical Sciences, 53(10) (2011) 886-896.

Power System Technology
ISSN:1000-3673
Received: 06-05-2024 *Revised: 15-06-2024* *Accepted: 28-07-2024*

[31]K. Swain, F .Mebarek-Oudina, S. Abo-Dahab, Influence of MWCNT/Fe 3 O 4 hybrid nanoparticles on an exponentially porous shrinking sheet with chemical reaction and slip boundary conditions, Journal of Thermal Analysis and Calorimetry, 147(2) (2022) 1561-1570.

[32]H. Yasmin, L.A. AL-Essa, R. Bossly, H. Alrabaiah, S.A. Lone, A. Saeed, A numerical investigation of the magnetized water-based hybrid nanofluid flow over an extending sheet with a convective condition: Active and passive controls of nanoparticles, Nanotechnology Reviews, 13(1) (2024) 20240035.

[33]D. Yang, S. Ahmad, K. Ali, S. Algarni, T. Alqahtani, W. Jamshed, S.M. Hussain, K. Irshad, H. Ahmad, CFD analysis of paraffin-based hybrid (Co–Au) and trihybrid (Co–Au–ZrO2) nanofluid flow through a porous medium, Nanotechnology Reviews, 13(1) (2024) 20240024.

[34]J.A. Khan, M. Mustafa, T. Hayat, A. Alsaedi, Three-dimensional flow of nanofluid over a non-linearly stretching sheet: An application to solar energy, International Journal of Heat and Mass Transfer, 86.164-158 (2015)

[35]R. Ahmad, M. Mustafa, Model and comparative study for rotating flow of nanofluids due to convectively heated exponentially stretching sheet, Journal of Molecular Liquids, 220 (2016) 635-641.

[36]A. Mushtaq, M. Mustafa, T. Hayat, A. Alsaedi, Numerical study for rotating flow of nanofluids caused by an exponentially stretching sheet, Advanced Powder Technology, 27(5) (2016) 2223-2231.

[37]T. Hayat, I. Ullah, T. Muhammad, A. Alsaedi, Magnetohydrodynamic (MHD) three-dimensional flow of second grade nanofluid by a convectively heated exponentially stretching surface, Journal of Molecular Liquids, 220 (2016) 1004-1012.

[38]M.I. Afridi, M. Qasim, S. Saleem, Second law analysis of three dimensional dissipative flow of hybrid nanofluid, Journal of Nanofluids, 7(6) (2018) 1272-1280.

[39]A. Hussain, M.H. Alshbool, A. Abdussattar, A. Rehman, H. Ahmad, T.A. Nofal, M.R. Khan, A computational model for hybrid nanofluid flow on a rotating surface in the existence of convective condition, Case Studies in Thermal Engineering, 26 (2021) 101089.